Journal of Alloys and Compounds 509 (2011) 6247–6251

Contents lists available at ScienceDirect

Journal of Alloys and Compounds

journal homepage: www.elsevier.com/locate/jallcom

Efficient cerium-based sol–gel derived phosphors in different garnet matrices for light-emitting diodes

Arturas Katelnikovas[a,c], Jonas Jurkevičius[b,*], Karolis Kazlauskas[b], Pranciškus Vitta[b], Thomas Jüstel[c], Aivaras Kareiva[a], Artūras Žukauskas[b], Gintautas Tamulaitis[b]

[a] Department of General and Inorganic Chemistry, Vilnius University, Naugarduko 24, LT-03225 Vilnius, Lithuania
[b] Semiconductor Physics Department and Institute of Applied Research, Vilnius University, Sauletekio 9, LT-10222 Vilnius, Lithuania
[c] Department of Chemical Engineering, University of Applied Sciences Münster, Stegerwaldstr. 39, D-48565 Steinfurt, Germany

ARTICLE INFO

Article history:
Received 27 October 2010
Received in revised form 3 March 2011
Accepted 4 March 2011
Available online 11 March 2011

Keywords:
Phosphors
Sol–gel processes
Optical properties
Luminescence

ABSTRACT

Efficiency of sol–gel derived $Y_{3-x}Al_5O_{12}:Ce_x^{3+}$ (YAG:Ce) and $Y_{3-x}Mg_2AlSi_2O_{12}:Ce_x^{3+}$ (YMASG:Ce) phosphors, which are prospective for application in white light emitting diodes (LED), is studied. Sets of samples containing different cerium amount x from 0.015 to 0.06 and sintered at different temperatures (1400–1550 °C) were investigated. Importance of absorption peculiarities in agglomerates of phosphor nanocrystals is demonstrated by studying the excitation wavelength dependence of quantum efficiency and by applying PL measurements in confocal mode. Emission saturation is demonstrated to occur at higher excitation intensities than those typical for operating white LEDs.

Good spectral matching of absorption band with the emission of the most efficient InGaN-based light emitting diodes (LEDs) emitting at 465 nm and high quantum efficiency (typically 77% [1]) put forward the YAG:Ce phosphors as the currently most efficient converters of the light emitted by InGaN-based LEDs into the yellow spectral region in white LEDs produced on commercial scale nowadays. Commercial phosphor conversion white LEDs with YAG:Ce as a single phosphor are quite efficient, but have high correlated color temperature (>5000 K) due to the lack of emission in the red region. Consequently, the color rendition ability of these daylight dichromatic LEDs is insufficient for general lighting and other lighting applications requiring high color fidelity [2].

The emission band of Ce^{3+} ions in a crystal matrix is red-shifted due to crystal field. The crystal field in a matrix with garnet structure can be increased by an increased diameter of the ion on the dodecahedral site. In contrast to that, an increased average diameter of the ions located onto the octahedral and/or tetrahedral sites results in an increase covalent interaction with surrounding oxygen anions and thus in less covalent interaction between the same oxygen anions and the ions located at the dodecahedral site [3,4]. This feature has been used to shift the YAG:Ce emission further to longer wavelengths by the partial substitution of Y^{3+} in the garnet lattice by Gd^{3+} [5,6] or Tb^{3+} [7,8]. However, the red shift achieved is not large enough to pay off, and this approach is not followed on commercial scale. Attempts to red-shift and broaden the emission band by the incorporation of N^{3-} ions into the coordination spheres of a part of Ce^{3+} ions (the source of N^{3-} was Si_3N_4) were successful, but efficiency of these phosphors is limited by strong concentration quenching of the low-energy Ce^{3+} ions with the modified coordination sphere [9]. In another approach, emission of Eu^{2+} ions in different matrices (chalcogenides [10–12], nitridosilicates [13–15], oxynitride [16,17]) has been employed. However, either low efficiency, structural instability, or high firing temperatures needed for synthesis or combinations of these drawbacks hinder a wide application of the Eu^{2+}-based red phosphors in dichromatic LEDs. Thus, improvement of the color rendition properties of dichromatic white LEDs without loosing their efficiency is still an open problem.

YAG:Ce phosphors for commercial LEDs are produced by an oxide melting process [18]. Meanwhile, inexpensive methods of YAG:Ce fabrication at reduced temperatures received increasing interest [19–22]. On one hand, these techniques are convenient for searching new matrices able to shift the Ce^{3+} emission band further to the red region. On the other hand, they are also prospective for commercial use due to the low cost of phosphor fabrication. However, the quantum efficiency of the YAG:Ce phosphors derived using these techniques is usually lower than that of the YAG:Ce phosphors produced by a oxide melting process [23].

Sol–gel technique has been successfully applied for the fabrication of YAG:Ce with a stable garnet phase [24]. Recently, stable garnet phase, high efficiency, and a substantial band shift to the red

* Corresponding author.
E-mail address: getjonas@gmail.com (J. Jurkevičius).

0925-8388/$ – see front matter © 2011 Elsevier B.V. All rights reserved.
doi:10.1016/j.jallcom.2011.03.032

region (emission peak position at ~610 nm) have been evidenced in sol–gel combustion derived $Y_{3-x}Mg_2AlSi_2O_{12}:Ce_x^{3+}$ (YMASG:Ce) phosphor [25,26]. Structural characteristics of the phosphor were reported in [26]. In this paper, we study the quantum efficiency of the sol–gel derived garnet phosphors YAG:Ce and YMASG:Ce containing different amounts of cerium ions and sintered at different temperatures. We demonstrate that red YMASG:Ce phosphors exhibit a very high quantum efficiency and are prospective for commercial use in white dichromatic LEDs with improved color rendition properties.

1. Experimental

A detailed synthesis descriptions can be found in our previous publications [24–26]. Briefly, sol–gel and sol–gel combustion techniques were employed in preparation of YAG:Ce and YMASG:Ce, respectively. Target materials were prepared from Y_2O_3 (99.999% ChemPur), $Ce(NO_3)_3{\cdot}6H_2O$ (99.9% ChemPur), $Mg(NO_3)_2{\cdot}6H_2O$ (≥98% Sigma–Aldrich), $Al(NO_3)_3{\cdot}9H_2O$ (≥98% Sigma–Aldrich), nano-scale SiO_2 (99.0% Merck), 1,2-ethanediol (≥99% Sigma–Aldrich), and tris(hydoxymethyl)-aminomethane (99.9% Merck).

In the sol–gel synthesis of YAG:Ce, yttrium oxide was dissolved in 0.2 M acetic acid solution. Then, stoichiometric amounts of aluminum and cerium nitrates were added. Furthermore, 1,2-ethanediol was added as a complexing agent and the resulting mixture was concentrated by slow evaporation at 65 °C under constant stirring. The obtained (Y,Ce)–Al–O acetate–nitrate–glycolate gels were oven (110 °C) dried, preheated at 800 °C for 2 h and subsequently sintered for 10 h at 1000 or 1300 °C in air.

In the sol–gel combustion synthesis of YMASG:Ce yttrium oxide was dissolved in hot diluted nitric acid and the solution was evaporated till dryness in order to remove an excess of nitric acid. The residue was dissolved in distilled water and stoichiometric amounts of aluminum, magnesium, cerium nitrates and silica were added. The obtained mixture were stirred for 1 h at 65–75 °C and tris(hydroxymethyl)-aminomethane was added with the molar ratio of 1:1 to all metal ions. The mixture was stirred for 1 h at the same temperature and, after concentrating by slow evaporation, the sols turned into transparent gels. Then, temperature was raised to 250 °C and self-maintaining gel combustion process, accompanied with evolution of large gas amount, started. The resulting black powders were oven (120 °C) dried, preheated at 900 °C for 2 h in air and subsequently sintered for 4 h at 1400–1550 °C under CO atmosphere. A corundum crucible was half filled with active carbon. Then, a smaller crucible with precursor was placed inside. The bigger crucible was closed and annealed.

Measurements of the photoluminescence quantum efficiency (QE) were carried out using an integrating sphere (*Sphere Optics*) and following the method suggested by de Mello et al. [27]. Briefly, the method allows determining the sample QE by measuring the ratio between the number of photons emitted (N_{em}) and the number of those absorbed (N_{abs}) by the sample using the relation

$$\mathrm{QE} = \frac{N_{em}}{N_{abs}} = \frac{I_{sample}}{I_{exc} - I'_{exc}} \quad (1)$$

where I_{sample} is the spectrally integrated photoluminescence (PL) intensity of the sample excited inside the sphere, I_{exc} indicates the integrated intensity of the excitation light with the sample being removed from the sphere, while I'_{exc} designates the integrated intensity of the excitation light with the sample being excited in the sphere. Since I_{exc} and I'_{exc} correspond to the number of photons incident on the sample and to the number of photons transmitted or reflected (i.e. not absorbed) by the sample, respectively, their difference equals the number of photons absorbed by the sample. Eq. (1) is a simplified expression of the one derived in Ref. [27] and is well suited for the determination of PL QE in small volume samples featuring a negligible absorption of the emitted light reflected from the sphere walls and redirected onto the sample.

InGaN LED with the emission band peaked at 440 nm was used as an excitation source. Sample PL and excitation light spectra were simultaneously registered using a spectrometer (*Hamamatsu PMA-11*) equipped with a back-thinned CCD and coupled to the integrating sphere by an optical fiber. A special transparent container was used to compress the powdered samples into homogeneous layers of a fixed thickness. Layer thickness was selected to avoid the possible influence of reabsorption on the emitted light. Before performing the routine measurements, otherwise identical samples of different thickness were prepared and QE of these samples was measured. The QE values measured in samples with thicknesses above ~0.2 mm decreased with increasing sample thickness, while no thickness dependence was observed below a thickness of 0.2 mm that was maintained further in all routine measurements reported here.

The use of an integrating sphere was crucial for reliability of the QE measurements in highly scattering powdered samples, since it allowed both the reflection and transmission coefficients to be taken into account simultaneously. Moreover, the obtained results were insensitive to the angular distribution of emitted light defined by the refractive index of the material, and to the orientation of the emitting dipoles within the sample. Although the integrating sphere method is an absolute method and requires no reference material of known QE for the determination of sample QE, the accuracy of our QE setup was verified by performing measurements with a reference. Quinine sulfate dissolved in 0.1 M H_2SO_4 and featuring QE of 53 ± 2.3% at an excitation wavelength of 366 nm served as a reference [28]. The excellent agreement of the estimated QE value with that reported for the reference ensured high reliability of the measurements.

Measurements of photoluminescence spectra with spatial resolution were carried out in confocal mode. A CW He–Cd laser emitting at 442 nm was used for excitation. Confocal microscope *Alpha* 300 S manufactured by *WITec* with high numerical aperture (NA = 0.9) objective was used and ensured in-plane spatial resolution of approximately 200 nm. For spectral resolution, the microscope was coupled by an optical fiber to a *Cromex* spectrometer followed by a thermoelectrically cooled CCD camera.

All experiments have been carried out at room temperature.

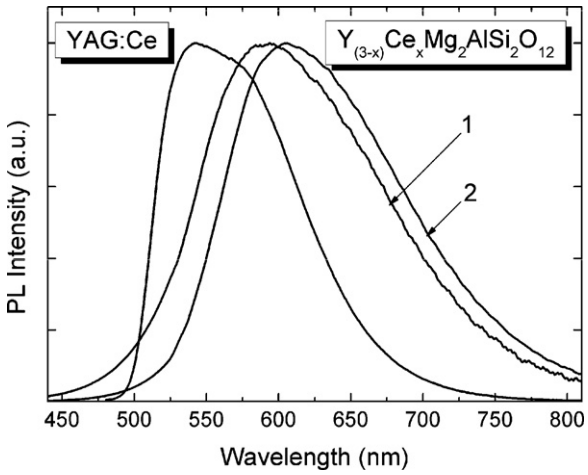

Fig. 1. Normalized PL spectra of $Y_{(3-x)}Ce_xMg_2AlSi_2O_{12}$ at $x = 0.015$, $T_S = 1400$ °C (1) and $x = 0.06$, $T_S = 1550$ °C (2), and YAG:Ce and under 440 nm excitation.

2. Results and discussion

As reported earlier [25,26], the PL spectrum of YMASG:Ce has one broad band, which consists of two strongly overlapping emission bands caused by optical transitions between the lowest excited 5d sublevel to 4f sublevels $^2F_{5/2}$ and $^2F_{7/2}$ of Ce^{3+} [29]. The PL spectrum is red-shifted in respect of the corresponding spectrum of Ce^{3+} in the YAG matrix. This redshift slightly increases with increasing cerium content (at least within the range from 0.015 to 0.06 studied in our experiments) and increasing sintering temperature (from 1400 to 1550 °C). The maximum difference in the red-shift observed (~15 nm) is illustrated in Fig. 1, where normalized PL spectra of $Y_{3-x}Mg_2AlSi_2O_{12}:Ce_x^{3+}$ samples with $x = 0.06$ and $T_S = 1550$ °C and with $x = 0.015$ and $T_S = 1400$ °C are depicted, together with a typical spectrum of YAG:Ce, for comparison.

The dependence of the QE of YAG:Ce phosphors sintered at two temperatures is presented in Fig. 2. The QE measured in the set of samples sintered at 1000 °C exhibits a monotonous decrease from 34% down to 14% with Ce content x increasing from 0.015 to 0.1. The QE for the set of samples sintered at 1300 °C is nearly the same both at low and high Ce content within the same range of x variation. However, the QE is bouncing up and down at $x = 0.06$ and 0.07, respectively. Similar bouncing at the same x values has been previously observed in YAG:Ce photoluminescence. Since a separate phase of crystalline oxide CeO_2 was observed in the XRD spectra of the samples exhibiting the bouncing, this behaviour has been attributed to the influence of this oxide phase [24].

YMASG:Ce with small Ce content exhibits high QE, which is comparable with the QE of the YAG:Ce phosphors fabricated using a similar sol–gel technique. The QE of $Y_{3-x}Mg_2AlSi_2O_{12}:Ce_x^{3+}$ with $x = 0.015$ is 31%, 33%, and 35%, for samples sintered at 1500 °C, 1450 °C, and 1400 °C, respectively. However, QE decreases substan-

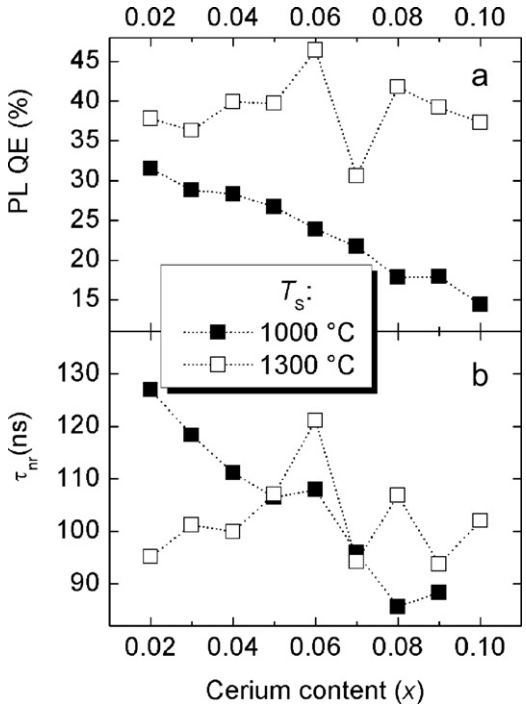

Fig. 2. Dependence of PL quantum efficiency (a) and carrier nonradiative recombination time (b) on cerium content in $Y_{3-x}Al_5O_{12}:Ce_x$ phosphors, sintered at different temperatures T_S, indicated.

tially when the cerium content is increased. This concentration quenching effect is demonstrated in Fig. 3(a). The samples sintered at 1500 °C, 1450 °C, and 1400 °C show a similar trend, though this decrease in QE is slightly more pronounced for the samples sintered at 1400 °C than that for those sintered at 1500 °C. Samples sintered at 1550 °C have considerably lower QE values and less pronounced dependence of QE on Ce concentration.

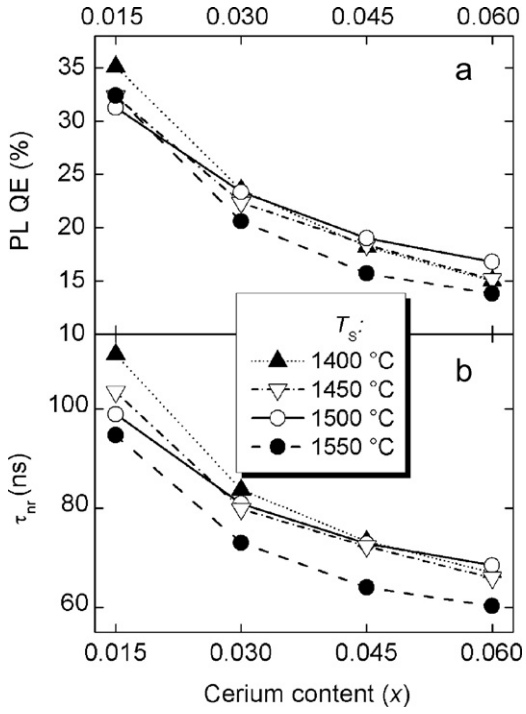

Fig. 3. Dependence of PL quantum efficiency (a) and carrier nonradiative recombination time (b) on cerium content in $Y_{3-x}Mg_2AlSi_2O_{12}:Ce_x$ phosphors, sintered at different temperatures T_S, indicated.

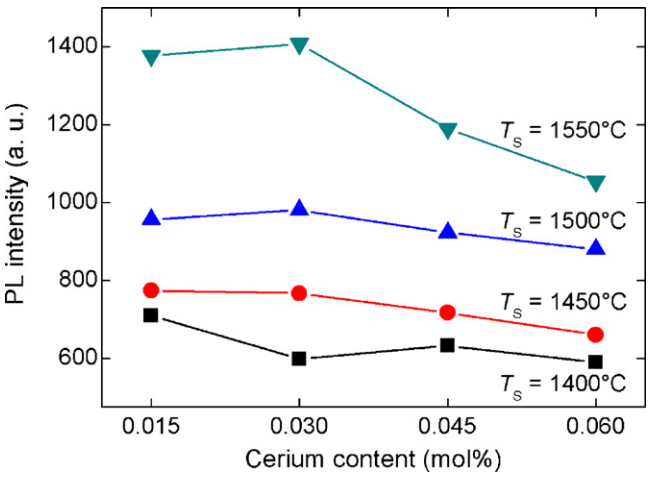

Fig. 4. Cerium content dependence of PL intensity of YMASG:Ce phosphor. Corresponding sintering temperatures are indicated.

The considerable drop in QE of YMASG:Ce phosphors with increasing Ce content is unfavorable for their applications requiring high emission power per volume of the phosphor. The origin of this drop is probably concentration quenching. This effect can be formally treated as an additional channel for nonradiative recombination. Concentration quenching decreases nonradiative recombination time and, consequently, QE. QE can be expressed through radiative and nonradiative recombination times, τ_r and τ_{nr}, respectively, as:

$$\mathrm{QE} = \frac{1}{(1+\tau_r)/\tau_{nr}} \tag{2}$$

Nonradiative recombination time can be extracted using QE and photoluminescence decay time τ_{PL}, which is a directly measurable parameter and is already reported for this set of samples [26]. Since the luminescence decay rate equals the sum of radiative and nonradiative recombination rates, the nonradiative recombination time τ_{nr} can be expressed as

$$\tau_{nr} = \frac{\tau_{PL}}{1-\mathrm{QE}} \tag{3}$$

The dependence of τ_{nr} on Ce content in YMASG:Ce phosphors is presented in Fig. 3(b). The dependence was calculated using Eq. (2), data on QE presented in Fig. 3(a), and data on τ_{PL} previously reported in Ref. [26]. Nonradiative recombination time is of the order of 100 ns in the samples with low Ce content and asymptotically approaches a value of ~60 ns at the further increase of Ce content.

The cerium content dependence of nonradiative recombination time extracted for YMASG:Ce phosphors can be compared with the corresponding dependence for YAG:Ce, which has been extracted using the same procedure and is presented in Fig. 2(b). The nonradiative recombination time of YMASG:Ce with small Ce content is similar with that for YAG:Ce phosphors, however, the concentration quenching proceeds faster in YMASG:Ce.

The PL intensity dependence on cerium content and sintering temperature of YMASG:Ce is presented in Fig. 4. Note that, despite a lower quantum efficiency, the samples subjected to higher sintering temperature exhibit a higher PL intensity. For example at $x = 0.015$, the PL intensity of the sample sintered at 1550 °C is twice as high as of the sample sintered at 1400 °C, though the QEs of the samples are 33% and 35%, respectively. Note also that the PL intensity decrease with increasing Ce content is more pronounced for samples sintered at a higher temperature.

The observed inconsistency between PL intensity and quantum efficiency can be explained by different absorption efficiency: the

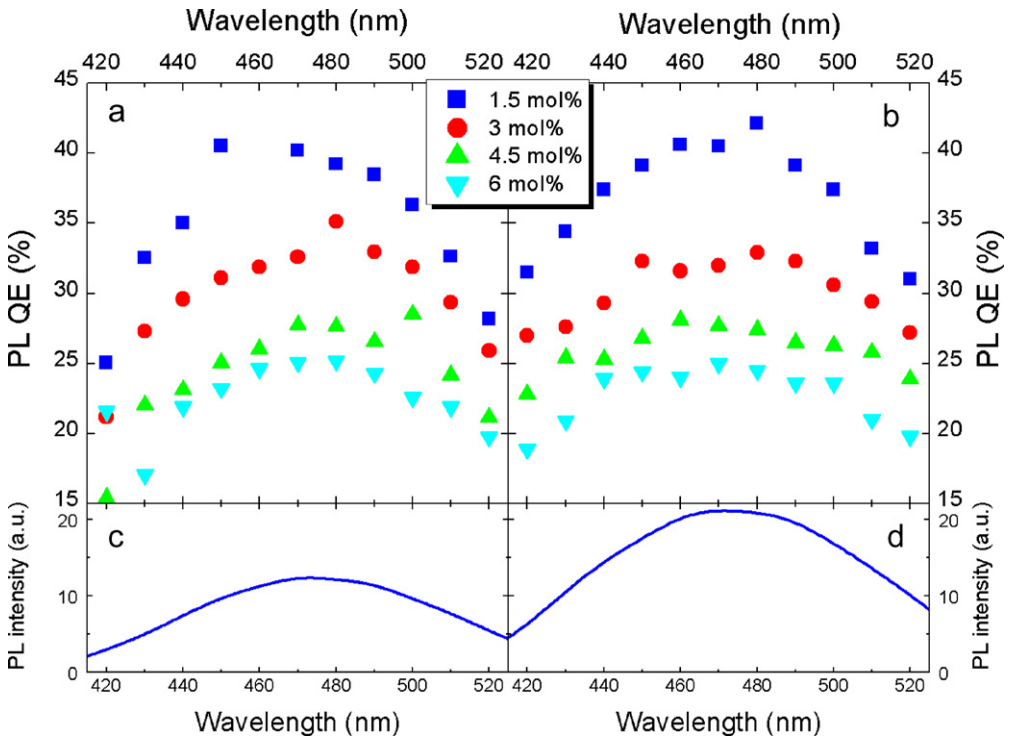

Fig. 5. Dependence of quantum yield on excitation light wavelength in YMASG:Ce phosphors sintered at 1400 °C (a) and 1550 °C (b), cerium content is indicated; luminescence excitation spectra of phosphors $Y_{2.985}Mg_2AlSi_2O_{12}:Ce_{0.015}$ sintered at T_S = 1400 °C (c) and T_S = 1550 °C (d).

absorption coefficient of samples sintered at higher temperatures is higher, thus the total PL intensity is higher in spite of their lower quantum efficiency. This feature has to be taken into account when optimizing the fabrication technology for practical applications.

The importance of absorption peculiarities has also been observed by studying the dependence of QE on the wavelength of light used for excitation. This dependence for two sets of YMASG:Ce samples sintered at different temperatures is presented in Fig. 5. The dependence has the shape of a band peaked at ~470 nm. The band shape basically coincides with the shape of the luminescence excitation spectrum reported in Ref. [25]. This is an indication that the absorption influences not only the emission intensity per volume (and, consequently, the PL intensity) but also QE, which generally should be constant: in the first approach, each excitation photon absorbed should result in emission of a PL photon with probability proportional to QE without any dependence on excitation wavelength.

The dependence of QE on excitation wavelength might be explained by absorption, scattering and escape of light in agglomerates of phosphor nanonocystals. Agglomerated morphology of the phosphor powder has been already reported in Ref. [26]. Light with the wavelength at the absorption band peak is absorbed predominantly in the nanocrystals located at the agglomerate surface. Meanwhile, absorption length increases for the wavelengths at the slopes of the absorption band. This light is more efficient for excitation of the interior of the agglomerate. Due to the stronger influence of reabsorption resulting in increased influence of nonradiative recombination, the escape probability of the light emitted in the interior of the agglomerate is lower than that for the light emitted close to the agglomerate surface. Thus, the resulting QE has a spectrum, which corresponds to the absorption spectrum.

To reveal the luminescence properties of the agglomerates we used PL spectroscopy in confocal mode enabling a spatial in-plane resolution of 200 nm. These measurements show that the grains consist of nanocrystals with diameters below 200 nm. Two images mapping the PL intensity (a) and peak wavelength (b) of a compact grain of the YMASG:Ce powder are presented in Fig. 6(a) and (b), respectively. The total diameter of the smallest grains is typically of ~1 μm, i.e. large enough for reabsorption to be important. The image demonstrates quite an ungradual spatial PL distribution: the intensity is high at the core of the grain and decreases quite abruptly on the grain edges.

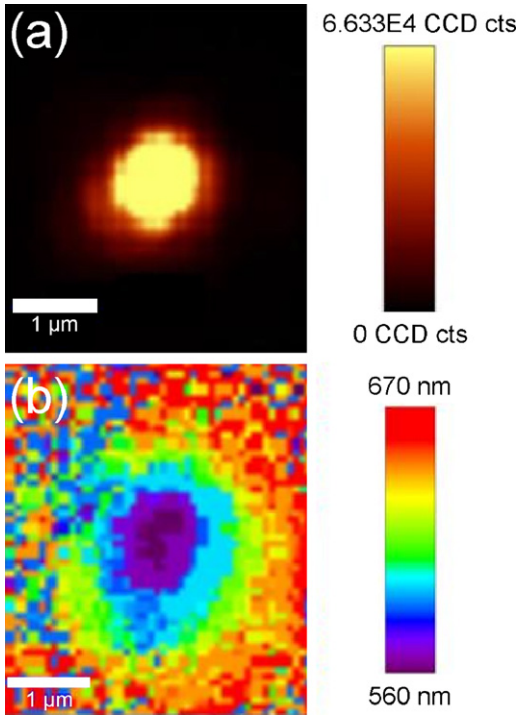

Fig. 6. Spatial distributions of luminescence intensity (a) and peak wavelength (b) of 1 μm sized YMASG:Ce phosphor grain under 441.6 nm excitation by He–Cd laser at power density of 3.5 MW/cm^2.

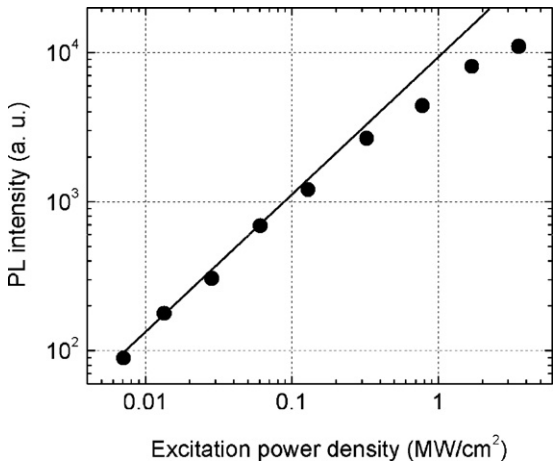

Fig. 7. Luminescence intensity dependence on excitation power density for phosphor $Y_{2.985}Mg_2AlSi_2O_{12}:Ce_{0.015}$ sintered at T_S = 1400 °C under excitation by 441,6 nm He–Cd laser.

Note that the PL peak at the edges of the agglomerate is red-shifted in respect to its position at the center. The same trend is also observed by scanning the agglomerate in direction perpendicular to the plane depicted in Fig. 6 (not shown in the figure). This can be explained by a different strain experienced by nanocrystals located at the surface and in the interior of the agglomerate.

The excitation intensity dependence of PL intensity has been investigated using confocal microscopy for small agglomerates selected from powders of different samples under study. No significant change in shape or shift in position of the emission bands has been observed. The PL intensity dependence on excitation power density is presented in Fig. 7. The dependence is linear at low excitation power densities but tends to saturate at pump intensities elevated above ~0.1 MW/cm^2. In real LEDs, however, the phosphors are typically subjected to excitation power density of the order of W/cm^2. Thus, no saturation should be expected when using the YMASG:Ce phosphors in white LEDs.

3. Conclusions

In conclusion, sol–gel derived YMASG:Ce phosphors exhibit a red shift in comparison with the conventional YAG:Ce phosphor and under excitation by blue InGaN LED have a quantum efficiency that is comparable to that of conventional YAG:Ce phosphor. In view of exploitation of this phosphor in white LEDs, a problem is the concentration quenching, which is more pronounced in this phosphor than in YAG:Ce. The total PL output of YMASG:Ce strongly depends not only on the quantum efficiency but also on the absorption peculiarities. Thus, absorption parameters have to be optimized for better performance in practical applications. PL saturation is observed well above the excitation power densities typical for the operation of white InGaN-based LEDs.

References

[1] S.C. Allen, A.J. Stecki, Appl. Phys. Lett. 92 (2008) 143309.
[2] A. Žukauskas, R. Vaicekauskas, M.S. Shur, J. Phys. D: Appl. Phys. 43 (2010) 354006.
[3] G. Blasse, A. Bril, J. Chem. Phys. 47 (1967) 5139.
[4] W.W. Holloway, M. Kestigian, J. Opt. Soc. Am. 60 (1969) 59.
[5] T.Y. Tien, E.F. Gibbons, R.G. DeLosh, P.J. Zacmanidis, D.E. Smith, H.L. Stadler, J. Electrochem. Soc. 278 (1973) 120.
[6] Y. Shimizu, K. Sakano, Y. Noguchi, T. Moriguchi, US Patent 5 998 925 (1999).
[7] F. Kummer, F. Zwaschka, A. Ellens, A. Debray, G. Waitl, EP. Patent 1 116 418 (2003).
[8] A.A. Setlur, A.M. Srivastava, H.A. Comanzo, G. Chandran, H. Aiyer, M.V. Shankar, S.A. Weaver, Proc. SPIE 5187 (2004) 142.
[9] A.A. Setlur, W.J. Heward, M.E. Hannah, U. Happek, Chem. Mater. 20 (2008) 6277–6283.
[10] R. Mueller-Mach, G.O. Mueller, Proc. SPIE 3938 (2000) 30.
[11] Y. Hu, W. Zhuang, H. Ye, S. Zhang, Y. Fang, X. Huang, J. Lumin 111 (2005) 139.
[12] X. Zhang, L. Liang, J. Zhang, Q. Su, Mater. Lett. 59 (2005) 749.
[13] H.A. Höppe, H. Lutz, P. Morys, W. Schnick, A. Seilmeier, J. Phys. Chem. Sol. 61 (2000) 2001.
[14] R. Mueller-Mach, G. Mueller, M.R. Krames, H.A. Höppe, F. Stadler, W. Schnick, T. Juestel, P. Schmidt, Phys. Stat. Sol. A 202 (2005) 1727.
[15] K. Uheda, N. Hirosaki, Y. Yamamoto, A. Naito, T. Nakajima, H. Yamamoto, Electrochem. Solid State Lett. 9 (2006) H22.
[16] J.W.H. van Krevel, J.W.T. van Rutten, H. Mandal, H.T. Hintzen, R. Metselaar, J. Solid State Chem. 19 (2002) 165.
[17] R.-J. Xie, N. Hirosaki, K. Sakuma, Y. Yamamoto, M. Mitomo, Appl. Phys. Lett. 84 (2004) 5404.
[18] G. Bogner, A. Debray, G. Heidel, K. Hoehn, U. Muller, P. Schlotter, Proc. SPIE 3621 (1999) 143.
[19] M. Veith, S. Mathur, A. Kareiva, M. Jilavi, M. Zimmer, V. Huch, J. Mater. Chem. 9 (1999) 3069.
[20] Y. Pan, M. Wu, Q. Su, Mater. Sci. Eng. B 106 (2004) 251.
[21] G. Xia, S. Zhou, J. Zhang, J. Xu, J. Cryst. Growth 279 (2005) 357.
[22] D. Jia, Y. Wang, X. Guo, K. Li, Y.K. Zou, W. Jia, J. Electrochem. Soc. 154 (2007) J1.
[23] D. Haranath, H. Chander, P. Sharma, S. Singh, Appl. Phys. Lett. 89 (2006) 173118.
[24] A. Katelnikovas, P. Vitta, P. Pobedinskas, G. Tamulaitis, A. Žukauskas, J.-E. Jørgensen, A. Kareiva, J. Cryst. Growth 304 (2007) 361.
[25] A. Katelnikovas, H. Bettentrup, D. Ulrich, S. Sakirzanovas, T. Jüstel, A. Kareiva, J. Lumin 129 (2009) 1356.
[26] A. Katelnikovas, T. Bareika, P. Vitta, T. Jüstel, H. Winkler, A. Kareiva, A. Žukauskas, G. Tamulaitis, Opt. Mater. 32 (2010) 1261.
[27] J.C. de Mello, H.F. Wittmann, R.H. Friend, Adv. Mater. 9 (1997) 230.
[28] M.J. Adams, J.G. Highfield, G.F. Kirkbright, Anal. Chem. 49 (1977) 1850.
[29] Ed.Sh. Shionoya, W.M. Yen, Phosphor Handbook, CRC Press, Boca Raton/Boston/London/New York/Washington DC, 1999.